Applied Surface Science 358 (2015) 137–145

Contents lists available at ScienceDirect

Applied Surface Science

journal homepage: www.elsevier.com/locate/apsusc

Mechanistic study of the visible-light-driven photocatalytic inactivation of bacteria by graphene oxide–zinc oxide composite

Dan Wu[a], Taicheng An[b,*], Guiying Li[b], Wei Wang[a,c,*], Yuncheng Cai[c], Ho Yin Yip[a], Huijun Zhao[d], Po Keung Wong[a,*]

[a] School of Life Sciences, The Chinese University of Hong Kong, Shatin, NT, Hong Kong, China
[b] State Key Laboratory of Organic Geochemistry and Guangdong Key Laboratory of Environmental Resources Utilization and Protection, Guangzhou Institute of Geochemistry, Chinese Academy of Sciences, Guangzhou 510640, China
[c] State Key Laboratory of Material Processing and Die & Mould Technology, Huazhong University of Science and Technology, Wuhan 430074, China
[d] Centre for Clean Environment and Energy, Gold Coast Campus, Griffith University, Queensland 4222, Australia

ARTICLE INFO

Article history:
Received 23 June 2015
Received in revised form 4 August 2015
Accepted 5 August 2015
Available online 8 August 2015

Keywords:
Visible-light-driven photocatalyst
Graphene oxide–zinc oxide composite
Bacterial inactivation
Photosensitizing mechanism

ABSTRACT

The visible-light-driven (VLD) photocatalytic activity of graphene oxide–zinc oxide (GO–ZnO) composite prepared by a simple hydrothermal method was evaluated toward the inactivation of *Escherichia coli* K-12. The results showed that GO–ZnO composite had excellent VLD photocatalytic bacterial inactivation activity, comparing with those of ZnO and GO, which was attributed to the strong interaction between ZnO and GO in the composite. Accordingly, an interaction induced VLD photocatalytic inactivation mechanism of the strong interaction of GO with ZnO within the GO–ZnO composite was proposed. GO served as a photosensitizer and facilitated the charge separation and transfer, thus boosted the massive production of reactive oxygen species such as $^{\bullet}OH_{bulk}$, which was identified as the major reactive species from conduction band of ZnO, and resulted in a remarkable enhancement of bacterial inactivation efficiency. Moreover, GO–ZnO composite showed obviously superior photocatalytic bacterial inactivation within 10 min under natural solar light irradiation, indicating that GO–ZnO composite has great potential in wastewater treatment and environmental protection.

1. Introduction

Currently, due to growing concerns about the emergence of worldwide microbiologically contaminated water sources, it is urgent to develop efficient and eco-friendly water disinfection techniques to eliminate pathogenic microorganisms. Alternative to the traditional disinfection methods, semiconductor photocatalysis has been considered as an effective water purification approach to various microbial contaminations [1,2].

Zinc oxide (ZnO), with a bandgap of 3.27 eV, is one of the most widely studied semiconductor photocatalyst that can only be activated by UV light. In order to effectively utilize energy of visible spectrum of sunlight or indoor artificial light, it is crucial to extend the photo-response range of ZnO to visible light (VL) in photocatalytic process. Recently, graphene or graphene oxide (GO) has attracted increasing attention due to their good electron conductivity, large specific surface area and high adsorption ability [3,4]. In particular, the oxygen functional groups on the surface of GO can act as active anchoring sites for photocatalyst fabrication [5–7]. Therefore, a variety of GO–ZnO composites are developed to extend their applications in photocatalysis, such as heavy metal reduction [8], air purification [9], dye degradation [10,11], and photodynamic therapy [12]. Unfortunately, very limited work focused on using GO–ZnO composites for VLD bacterial inactivation.

Various reactive oxygen species (ROSs), such as superoxide radicals ($^{\bullet}O_2^-$), hydroxyl radicals in solution ($^{\bullet}OH_{bulk}$), and hydrogen peroxide (H_2O_2) are believed to be responsible for the destruction of microorganisms [13,14]. However, there are significant differences in VLD photocatalytic mechanisms for bacterial disinfection and other photocatalytic processes. Which ROS(s) plays the major role(s) for GO–ZnO composite in VLD photocatalytic bacterial inactivation process is still unclear. Although enhanced bacterial inactivation of GO–ZnO composites has been reported [15,16], the VLD charge transfer process between GO and ZnO and the role of GO in GO–ZnO composite still have not yet been identified. The enhanced photocatalytic activities of GO–ZnO composites in various pioneering studies were generally accepted to be attributable to the electron transfer ability of GO [8–12], which would facilitate the separation and transfer of photogenerated charges.

* Corresponding authors.
E-mail addresses: antc99@gig.ac.cn (T. An), weiwang@hust.edu.cn (W. Wang), pkwong@cuhk.edu.hk (P.K. Wong).

http://dx.doi.org/10.1016/j.apsusc.2015.08.033
0169-4332/

More recently, much effort has been made to endow wide-bandgap semiconductors (such as TiO_2, ZnS and ZnO) with VLD photocatalytic performances by using GO as a photosensitizer [17–21]. These results may provide a meaningful hint to better explain VLD photocatalytic bacterial inactivation mechanism of GO–ZnO composite. Hence, the detail VLD photocatalytic processes and mechanisms for bacterial disinfection are required a more systematic study.

In this study, the VLD photocatalytic inactivation activity of GO–ZnO composite photocatalysts toward a model bacterium, *Escherichia coli* K-12, was assessed. The role of GO in the GO–ZnO composites was explored to specify major/dominant reactive species involved in the inactivation process. Accordingly, a reasonable mechanism was also proposed to well explain the efficient VLD bacterial inactivation performance of prepared GO–ZnO composite photocatalyst. The GO–ZnO composite was also applied to measure the bacterial inactivation under natural solar light radiation.

2. Experimental

2.1. Synthesis of graphene oxide–zinc oxide (GO–ZnO) composite

Graphene oxide (GO) was prepared according to the modified Hummer's method [22]. The graphene oxide–zinc oxide (GO–ZnO) composite was synthesized by a simple hydrothermal method described as following: Typically, 5 mL GO aqueous solution (1 mg mL^{-1}) was added to 35 mL deionized (DI) water containing 0.5 g ZnO nanoparticles (NPs) (<100 nm, Sigma–Aldrich) (GO:ZnO = 1% weight ratio) and then kept stirring for 30 min. After that, the solution was transferred to 100 mL Teflon-sealed autoclave and maintained at 160 °C for 12 h. After cooling to the room temperature (~25 °C), the precipitate was centrifuged, washed with DI water and then 100% ethanol for several times, and finally dried at 60 °C in an oven. All the chemicals used in the experiments were of reagent grade and used as received without further purification.

2.2. Characterizations of GO–ZnO composite

The X-ray diffraction (XRD) pattern of as-prepared composites was performed using a SmartLab X-ray diffractometer (Rigaku, Tokyo, Japan) operating at 40 mA and 40 kV using Cu Kα as radiation source. Transmission electron microscopic (TEM) images were observed using Tecnai G2 Spirit transmission electron microscope (FEI, Hillsboro, OR, USA) at 200 kV equipped with an energy-dispersive X-ray (EDX) spectrometer. UV–vis diffuse reflectance spectra (DRS) were measured with a Varian Cary 500 UV–vis spectrophotometer (Palo Alto, CA, USA) equipped with a Labsphere diffuse reflectance accessory. X-ray photoelectron spectroscopy (XPS) experiments were recorded on an AXIS-ULTRA DLD-600W X-ray photoelectron spectrometer (Shimadzu-Kratos, Kyoto, Japan) using Al-Kα radiation as the excitation source. The Brunauer–Emmett–Teller (BET) specific surface area of the samples was determined with an ASAP 2020 volumetric adsorption analyzer (Micromeritics, Norcross, GA, USA). The Raman spectra were measured using a Renishaw RM 1000 Raman spectrometer (Wotton-under-Edge, UK) with the excitation of a 514 nm laser beam. The electrochemical impedance spectroscopy (EIS) measurements were performed with a CHI760C electrochemical working station (CH Instruments, Shanghai, China) in a three-electrode quartz cells with 0.1 M Na_2SO_4 electrolyte solution. The working electrode was obtained by the ZnO, GO and GO–ZnO composite samples deposited on a fluorinated-tin-oxide (FTO) conducting glass. Ag/AgCl and Pt served as the reference and the counter electrode, respectively.

2.3. Photocatalytic inactivation activity of GO–ZnO composite

The VLD photocatalytic inactivation of *E. coli* K-12 was conducted using fluorescent tubes (15 W, FSL, Foshan, China) as VL source. The VL intensity was measured by a LI-250 light meter (LI-COR, Lincoln, Nebraska, USA) and was fixed at 8.5 mW cm^{-2}. The cells of *E. coli* K-12 were inoculated into 50 mL of Nutrient Broth (Lab M, Lancashire, UK) at 37 °C for 15 h in a shaking incubator. The cultures were then washed twice with sterilized saline (0.9% NaCl) solution by centrifugation for 1 min, and then the cell pellet was re-suspended in sterilized saline solution. The final cell density was adjusted to about 1×10^7 colony forming unit (CFU) mL^{-1}. A suspension (50 mL) containing the photocatalyst (50 mg) and the bacterial cells in a 150 mL flask was kept at 25 °C with continuous stirring. At different time intervals, aliquots of the sample were collected and serially diluted with sterilized saline solution. 0.1 mL of the diluted sample was immediately spread on Nutrient Agar (Lab M, Lancashire, UK) plates and incubated at 37 °C for 24 h to determine the number of survival cells (in CFU). The detection limit was 1 CFU mL^{-1}. For comparison, dark (photocatalyst and bacterial cells without light) and light (bacterial cells and light without photocatalyst) controls were also included in the study. To identify the major reactive species accounting for the photocatalytic inactivation of *E. coli* K-12, specific scavenger at optimized concentration was added under otherwise identical conditions mentioned above. All the above experiments and controls were conducted in triplicates.

The bacterial cells and the photocatalyst mixture was collected before and after photocatalytic treatment, and stained with the dyes of LIVE/DEAD BacLight Bacterial Viability Kit (L7012, Molecular Probes, Inc., Eugene, Oregon, USA) following the procedure recommended by the manufacturer. After incubation at 25 °C in the dark for 15 min, the samples were transferred to a coverslip and examined under a ECLIPSE 80i fluorescence microscopy (Nikon, Tokyo, Japan) equipped with a filter block NUV-2A consisting of excitation filter Ex 400-680 (Nikon, Tokyo, Japan) and Spot-K slider CCD camera (Diagnostic Instruments Inc., Sterling Heights, Michigan, USA).

2.4. Detection of hydrogen peroxide (H_2O_2), hydroxyl radical ($^{\bullet}OH$) and superoxide ($^{\bullet}O_2^-$)

H_2O_2 produced during the photocatalytic inactivation was analyzed by a highly sensitive fluorometric method [23]. Briefly, 0.4 mL of the samples, 0.1 mL of $FeSO_4$ (0.25 mM) and 0.1 mL of coumarin (0.5 mM) were added into 0.4 mL of citrate buffer (pH 3) with further standing for 10 min. Then the mixture was measured at emission wavelength of 456 nm with excitation wavelength of 346 nm by an Infinite® M200 microplate reader (Tecan, Männedorf, Switzerland). The concentration of produced H_2O_2 was calculated based on the standard as the same procedure using pure H_2O_2 as the reference.

To detect the production of $^{\bullet}OH$, 50 mg GO–ZnO composite was suspended in a 50 mL saline solution containing terephthalic acid (TA) (5×10^{-4} M) and NaOH (2×10^{-3} M) [14]. The resulting suspension was then exposed to VL irradiation. At regular intervals, 1 mL the suspension was collected and centrifuged to separate the photocatalyst. Finally, fluorescence of the solution was measured at emission wavelength of 426 nm by exciting wavelength at 315 nm by the Infinite® M200 microplate reader.

To detect the production of $^{\bullet}O_2^-$, the procedure was similar to that of $^{\bullet}OH$ with nitroblue tetrazolium (NBT) instead of TA and NaOH [14]. The production of $^{\bullet}O_2^-$ was quantitatively analyzed by detecting the decrease of the concentration of NBT at

wavelength 259 nm with a LabTech Bluestar A UV–Vis spectrophotometer (Tianjing, China).

3. Results and discussion

3.1. Characterizations of photocatalysts

Fig. 1a shows the XRD patterns of GO, ZnO and GO–ZnO composite. The pattern of GO has a typical characteristic peak at $2\theta = 8.9^{\circ}$, corresponding to (001) inter-planar spacing (d-spacing) of about 1 nm, demonstrating the successful introduction of oxygen-containing groups on the basal plane compared to graphite (Fig. S1). The GO–ZnO composite showed similar XRD patterns as compared to pure ZnO. All the diffraction peaks can be well indexed to the hexagonal phase of ZnO (JCPDS 01-075-0576). Notably, no diffraction peaks of GO can be observed in the GO–ZnO composite, which may be ascribed to the low content and relatively low diffraction intensity of GO in the composites [6]. The morphologies of GO, ZnO and GO–ZnO composite are revealed through TEM analysis (Figs. S2 and 1b). As shown in Fig. 1b, the GO–ZnO composite presents similar size and morphology as the pure ZnO (Fig. S2b). However, both the edges of GO and ZnO were clearly observable in the GO–ZnO composite, suggesting that a good contact was formed between GO and ZnO.

XPS and Raman spectra were used to investigate the interfacial character as well as the interaction between GO and ZnO in the GO–ZnO composite. As shown in Fig. 2a, the C 1s spectrum of GO suggested the abundance of various oxygen-containing functional groups on the GO surface. The deconvoluted peaks centered at 284.4, 285.3, 287.2 and 288.9 eV were assigned to C—C, C—O, C═O and C(O)OH bonds, respectively [5]. As for GO–ZnO composite, the oxygen-containing functional groups in C 1s spectra exhibited smaller relative contents (Table S1), indicating the removal of oxygen-containing functional groups and partially reduction of original GO during the hydrothermal treatment. Meanwhile, it could be found a peak shift of the binding energies of C—C and C═O bonds in GO–ZnO composite (Fig. 2b), which implied that the strong interaction existed between ZnO and the oxygen-containing functional groups onto the GO surface [7]. In Fig. 2c, the binding energy peaks at 1021.6 and 1044.7 eV matched well with those of respective Zn $2p_{3/2}$ and Zn $2p_{1/2}$, which corresponded to the chemical element state of Zn^{2+} in ZnO and GO–ZnO composite. It was seen that the peak positions of Zn 2p of GO–ZnO composite was identical to those of ZnO, which confirmed that no chemical Zn–C bond was formed in the composite [24]. Raman spectra of GO and GO–ZnO composite were presented in Fig. 2d. GO displayed two typical bands located at 1357 cm^{-1} for D band and 1603 cm^{-1} for G band. The D band is ascribed to edge or in-plane sp^3 defects and disordered carbon, whereas the G band arises from in-plane vibration of ordered sp^2-bonded carbon atoms in a two dimensional hexagonal lattice [11]. In general, the I_D/I_G intensity ratio is a measure of the relative concentration of local defects/disorders and average size of the sp^2 domains in graphite materials [7]. Particular note was the I_D/I_G ratio increased to 0.90 for GO–ZnO composite as compared with 0.76 of GO, indicating the formation of the defects and disorders as well as a decrease in the average size of the sp^2 domains resulting from the removal of oxygen-containing functional groups, which corresponded to the results of XPS. Additionally, the D band for GO–ZnO composite showed a blue shift (1350 cm^{-1}) as compared with ZnO (1357 cm^{-1}), further implying a close interaction between ZnO NPs and GO sheets [25]. Therefore, the results of XPS and Raman spectra excluded the formation of Zn-C bond and all the above analyses illustrated the existence of a strong interaction between GO and ZnO within obtained composite. During hydrothermal process, the decrease of oxygen-containing functional groups resulted in some π electrons of C atom that cannot bond with others to form a delocalized large π bond. The remaining unpaired π electrons could easily bond with Zn atoms on the surface of ZnO in the GO–ZnO composite to form a strong interaction between GO and ZnO [24], which was expected to favor the charge transfer process.

The interface charge separation efficiency which would significantly affect the photocatalytic activity can be investigated by the electrochemical impedance spectra (EIS), and the results are presented in Fig. 3. The impedance spectra with a semicircle arc were observed at higher frequencies, corresponding to the kinetic control of the charge transfer process. The arc radius in EIS reflects the interface layer resistance arising at the surface of the electrode. The smaller arc radius implies the higher charge transfer efficiency [5]. The arc radius of GO–ZnO composite was smaller than that of ZnO under VL irradiation (Fig. 3a) or in dark (Fig. 3b). This suggested that the GO–ZnO photocatalysts had lower resistance than that of ZnO, implying that the mobility of charges separation and transfer at the solid–liquid interface was promoted. Furthermore, faster transient photocurrent response for GO–ZnO composites was observed compared to those of ZnO and GO (Fig. S3). The photocurrent enhancement after GO introduction suggested a higher separation efficiency of photogenerated electrons and holes, which could be assigned to the interaction of GO and ZnO in GO–ZnO composites. The result further demonstrated that the introduction of GO was beneficial for achieving efficient carrier transport and separation, which was highly desired for photocatalytic performance of prepared GO–ZnO composite.

The adsorption range of light of photocatalysts also plays an important role in the photocatalytic process, which can be examined by UV–vis diffuse reflectance spectroscopy (DRS). As shown in Fig. 4a, it can be seen that the addition of GO into composite significantly affected the light adsorption as well as the optical property of ZnO. An enhanced absorbance was observed at the VL region ($\lambda > 400$ nm), which was attributed to the broad background adsorption of GO within VL region. The Kubelka–Munk method was employed to determine the band gap of as-prepared photocatalysts (Fig. 4b), from which the band gap of the samples were estimated to be 3.13 and 3.15 eV, corresponding to GO–ZnO and ZnO, respectively. This similar value demonstrated that the strong interaction with GO hardly affected band gap of ZnO in GO–ZnO composite.

3.2. Photocatalytic inactivation activity

E. coli K-12, a common water-borne bacterium, was chosen as a representative microorganism to evaluate the VLD photocatalytic inactivation activity of GO–ZnO composite. In the dark and light control experiments, the bacterial population remained unchanged even after 60 min, indicating no toxic effect of GO–ZnO to the cells of *E. coli* K-12, and no photolysis of bacterial cells occurred under VL irradiation. As shown in Fig. 5a, no decrease of cell density was observed over the pure GO or ZnO irradiated by VL, implying that ZnO and GO themselves could not directly act as VLD photocatalysts for the bacterial inactivation. However, the GO–ZnO composite with 1 wt% GO loading exhibited the optimized photocatalytic inactivation (Fig. S4), with 1×10^7 CFU mL^{-1} of *E. coli* K-12 complete inactivation within 60 min under VL irradiation. It should be noted that the cell density was almost stable at 7-log in the first 30 min. This initial decay period was attributed to the accumulation of reactive species, since they were insufficient to engender remarkable bacterial damage [26]. In addition, the simple mixture of ZnO and GO did not have any detectable VLD photocatalytic activity toward the bacterial cells within 60 min (Fig. 5b), further suggesting the interaction between GO and ZnO was important in enhancing the overall VLD bacterial inactivation by GO–ZnO composite.

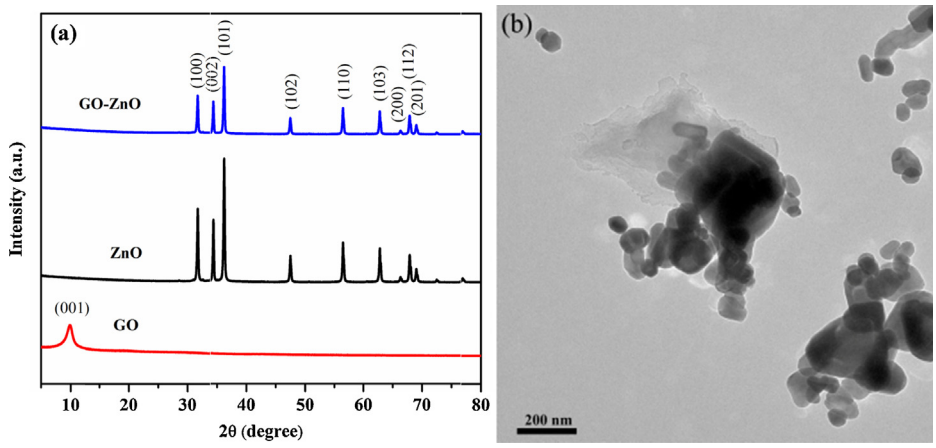

Fig. 1. (a) XRD patterns of GO, ZnO and GO–ZnO composite; (b) TEM image of GO–ZnO composite.

To study the cell membrane integrity of *E. coli* K-12 during photocatalytic inactivation by GO–ZnO composite, the fluorescent microscopic method was conducted according to previous study [26]. Once bound to a nucleic acid, membrane-permeable SYTO 9 emits green light while membrane-impermeable propidium iodide (PI) emits red light. Live bacterial cells with intact cell membranes are therefore stained fluorescent green, whereas dead bacterial cells with damaged cell membranes are stained fluorescent red. As shown in Fig. 6a, the viable cells presented intense green fluorescence. Notably, GO–ZnO composite could not been

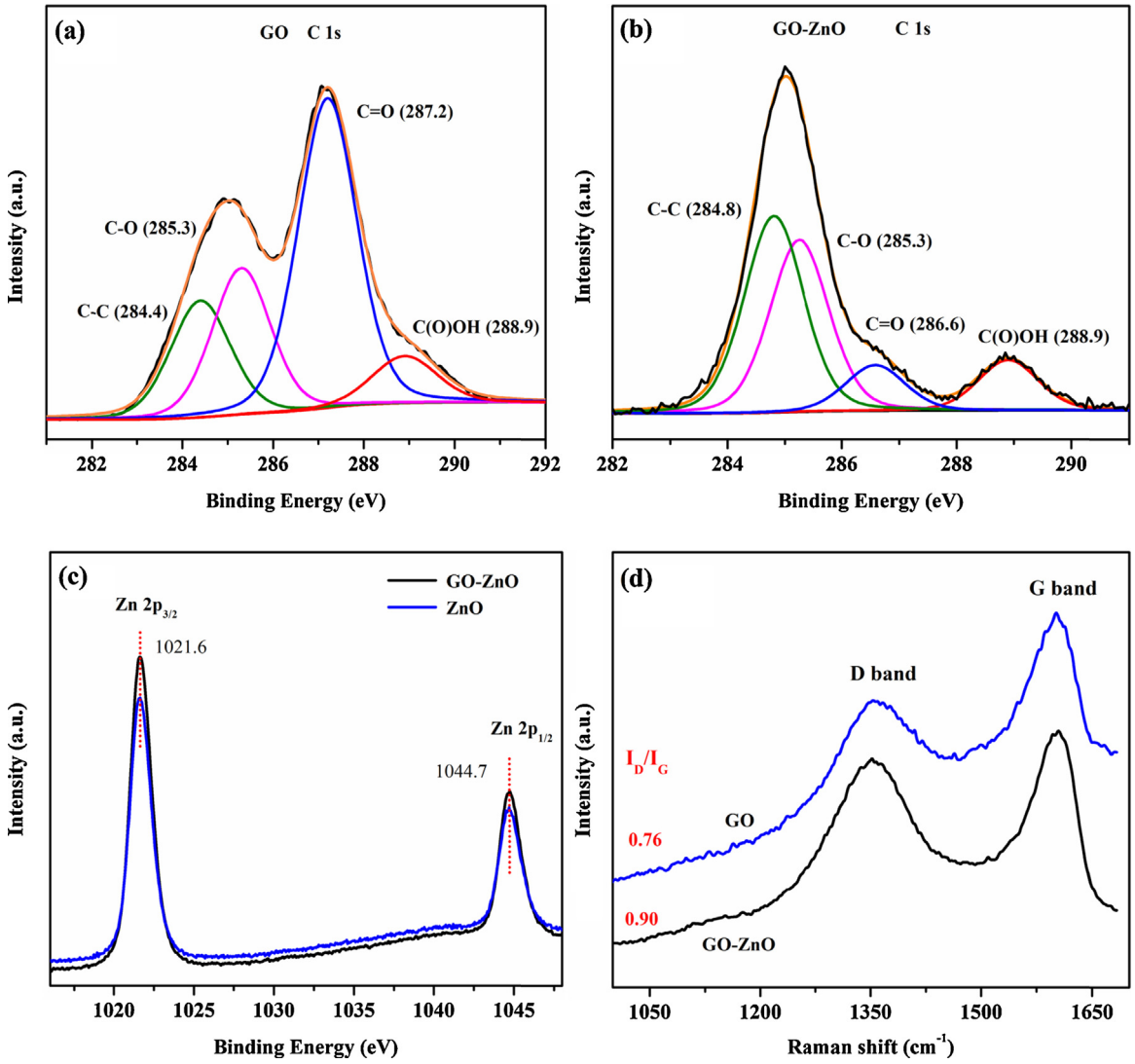

Fig. 2. XPS spectra of C 1s for (a) GO, (b) GO–ZnO composite, and (c) Zn 2p; (d) Raman spectra of GO and GO–ZnO composite.

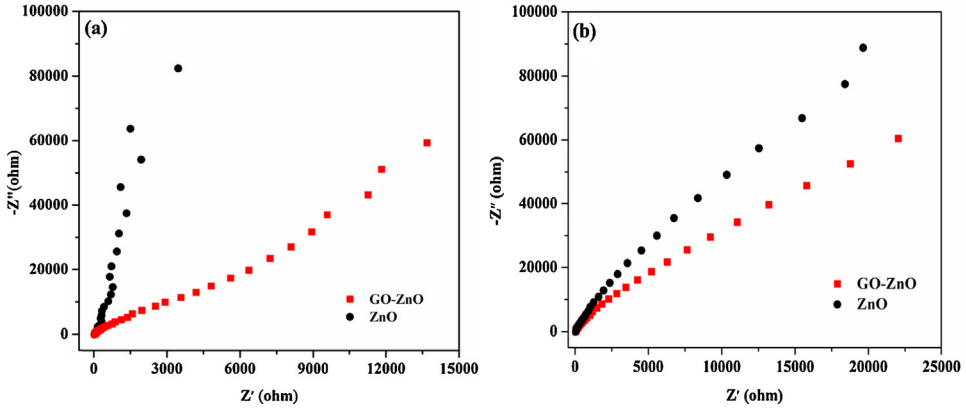

Fig. 3. EIS Nynquist plots of GO–ZnO composite and pure ZnO (a) under VL light irradiation and (b) in dark. (Na_2SO_4 = 0.1 M).

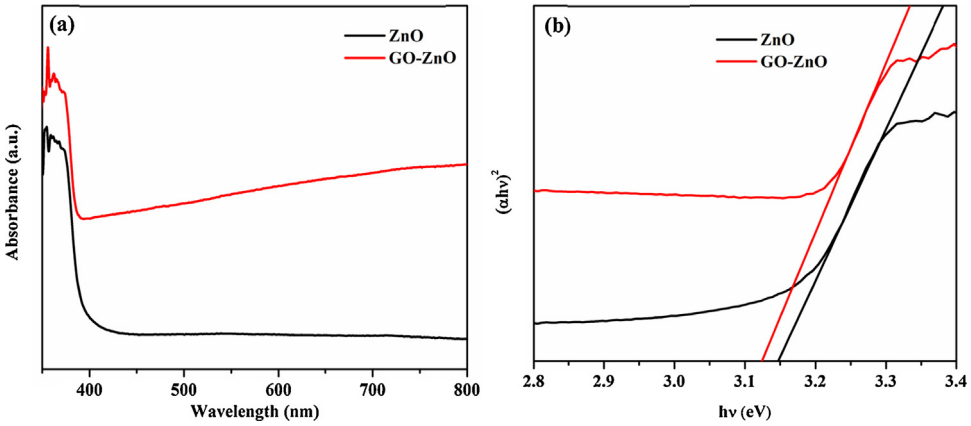

Fig. 4. (a) UV–vis diffuse reflectance spectra (DRS) of ZnO and GO–ZnO composite; (b) the plots of transformed Kubelka–Munk function *versus* the energy of visible light.

stained by neither SYTO 9 nor PI, and there was no obvious interaction between bacterial cells and the composite photocatalysts (Fig. 6b). After VLD photocatalytic treatment for 20 min, a portion of bacterial cells turned to red fluorescence (Fig. 6c), indicating these cells loss their cell membrane integrity. As time progressed, increasingly more red-stained bacterial cells were observed (Fig. 6d and e). Hence, the fluorescence microscopic observations provided direct evidence of bacterial cell membrane were damaged during photocatalytic process. The cell membrane is a protecting barrier and regulates the enzymatic reactions, cell recognition and substrate transport, thus controlling overall cell metabolism [27]. Cell membrane integrity is a primary indicator when bacterial cells are under adverse stress [28]. Therefore, it could be concluded that the GO–ZnO composite photocatalysts irradiated by VL led to progressive damage of the cell membranes of bacterial cells.

3.3. Mechanism of VLD photocatalytic inactivation

To further investigate the photocatalytic inactivation mechanism, the scavenger study, which employing different compound individually to remove the specific reactive species [14,26], was conducted in the photocatalytic inactivation process. Before

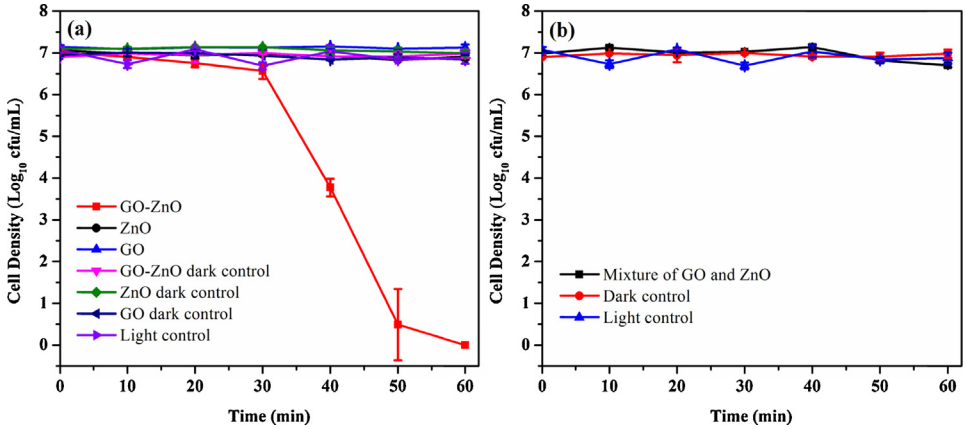

Fig. 5. Photocatalytic inactivation efficiency of *E. coli* K-12 (1×10^7 CFU mL^{-1}) in the presence of (a) GO–ZnO composite, GO (0.01 mg mL^{-1}) and ZnO and (b) simple mixture of ZnO and GO under VL irradiation provided by fluorescence tubes.

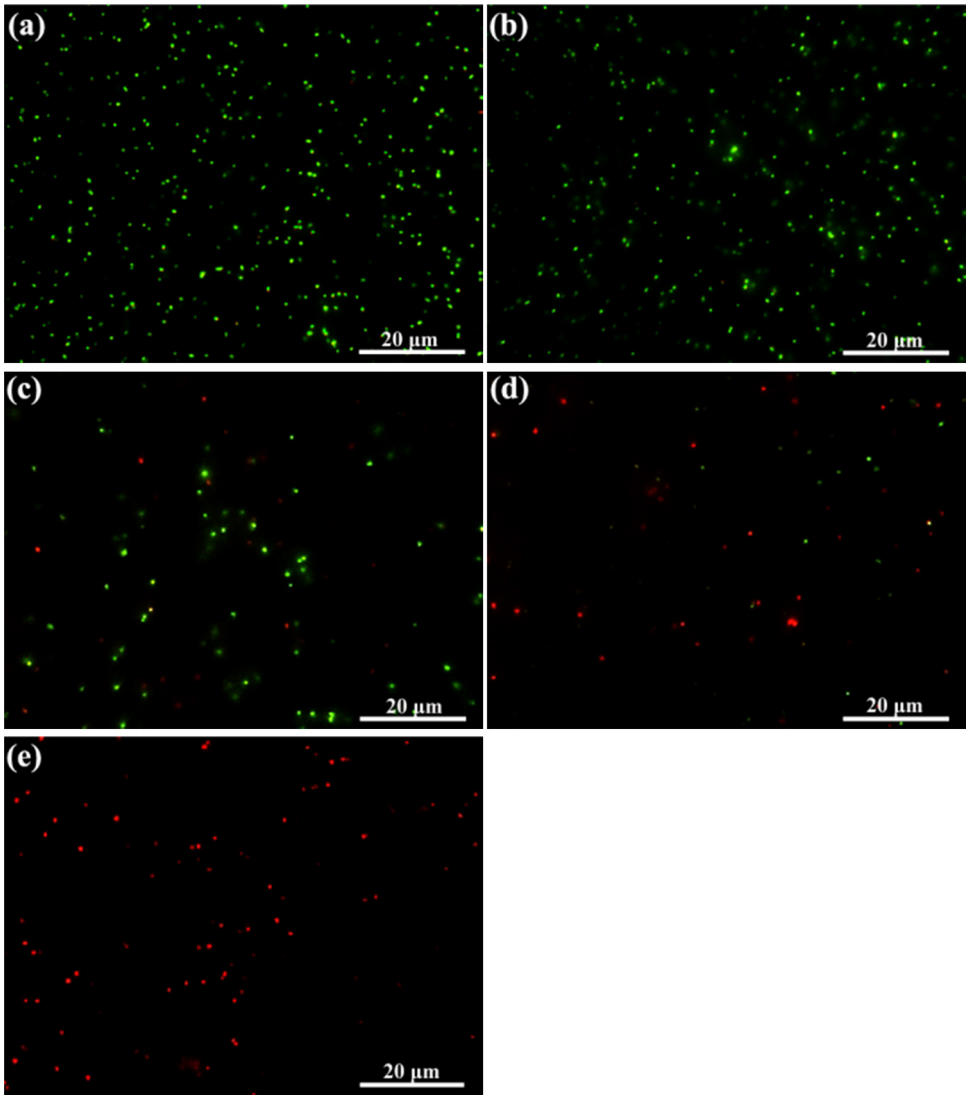

Fig. 6. Fluorescence microscopic images of *E. coli* K-12 after the photocatalytic treatment in the presence and in the absence of GO–ZnO composite under VL irradiation provided by fluorescence tubes. (a) *E. coli* K-12. The mixture of GO–ZnO composite and *E. coli* K-12 under VL irradiation for (b) 0, (c) 20, (d) 40, and (e) 60 min.

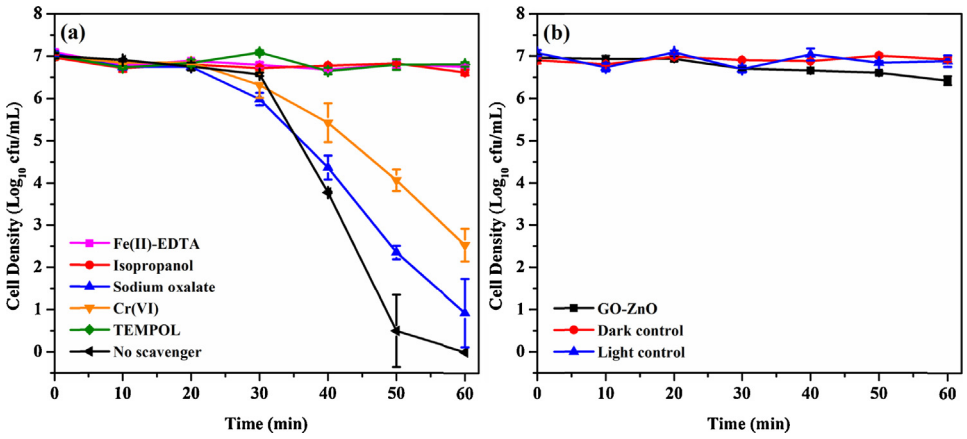

Fig. 7. The photocatalytic inactivation of *E. coli* K-12 (a) in the presence or absence of different scavengers: no scavenger, 5 mM isopropanol, 2 mM TEMPOL, 0.5 mM sodium oxalate, 0.1 mM Fe(II)-EDTA and 0.05 mM Cr(VI); and (b) argon aeration with GO–ZnO under VL irradiation provided by fluorescence tubes.

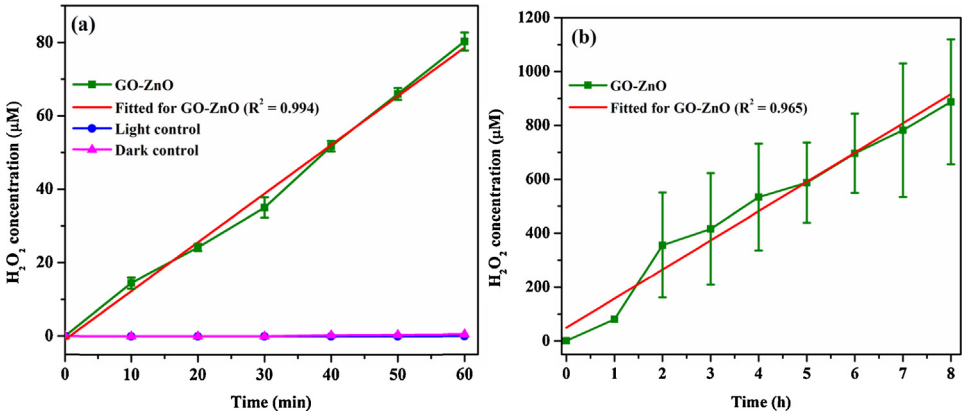

Fig. 8. H_2O_2 produced during the photocatalytic inactivation process with GO–ZnO under VL irradiation provided by fluorescence tubes (a) for 60 min and (b) for 8 h.

conducting the scavenging experiments, the applied concentrations of each scavenger were optimized to achieve their maximum scavenging effect but not cause toxicity to bacterial cells. As shown in Fig. 7a, with the addition of sodium oxalate as a scavenger for h^+, the inactivation efficiency had a negligible change compared with that without scavenger added, indicating h^+ was not the major reactive species in this VLD photocatalytic inactivation process. This is because GO–ZnO composite cannot be photoexcited by VL irradiation due to its wide bandgap and no e^- and h^+ were generated from ZnO. However, obvious inhibition effect of bacterial inactivation was observed when Cr(VI) was used to scavenge e^-, implying that e^- or its later resulted species was involved in the process of the photocatalytic inactivation, since other ROSs, such as $^\bullet O_2^-$, $^\bullet OH_{bulk}$ and H_2O_2 may be also formed from the reactions with e^- during the photocatalysis. Surprisingly, the photocatalytic inactivation was completely inhibited in the presence of isopropanol, Fe(II)-ethylenediaminetetraacetic acid (EDTA), and 4-hydroxy-2,2,6,6 tetramethyl-piperidinyloxy (TEMPOL) to remove $^\bullet OH$, H_2O_2, and $^\bullet O_2^-$, respectively. Since $^\bullet O_2^-$ was generally produced from e^-, while H_2O_2 and $^\bullet OH_{bulk}$ could be generated from both e^- in the CB and h^+ in the VB, argon (Ar) was aerated continuously in the reaction solution to remove O_2 and hence eliminated any influencing of ROSs produced from the e^- in CB, leaving only the h^+ in VB to be function to produce ROSs. As illustrated in Fig. 7b, with VL irradiation, GO–ZnO composite exhibited almost no bacterial inactivation, further confirming no h^+ in VB of ZnO was generated, since neither GO–ZnO composite nor ZnO was with VL response. This result also suggested that H_2O_2 and $^\bullet OH_{bulk}$ were probably produced from the e^- in CB rather than h^+ in VB. In CB, $^\bullet O_2^-$ is formed firstly to be activated the ambient molecular oxygen by reacting with e^-, while H_2O_2 is produced by the reduction or disproportionation of $^\bullet O_2^-$ [29], and then further forming $^\bullet OH_{bulk}$. The quenching of $^\bullet O_2^-$ and H_2O_2 would also decrease the amount of $^\bullet OH_{bulk}$, thus resulting in a significant inhibition effect on the inactivation efficiency.

To further investigate the major reactive species, the effect of direct contact between GO–ZnO photocatalyst and bacterial cell was also validated. A partition system was employed to separate the bacterial cell from the photocatalyst (Fig. S5) [29]. The semipermeable membrane (Molecular weight cutting limit is 12,000–14,000 Da) used in the partition system only allowed entry of $^\bullet OH_{bulk}$ and H_2O_2 [29], but prevented the passage of GO–ZnO composite (50–200 nm) and the cell of *E. coli* K-12, which has with molecular weight of about 2.6×10^6 Da. Thus, the direct contact between bacterial cell and GO–ZnO was prohibited. Expectedly, the GO–ZnO composite could completely photocatalytic inactivation of the bacterial cells within 6 h under VL irradiation in the partition system (Fig. S6), further confirming the existence of diffusible ROSs such as $^\bullet OH_{bulk}$ and H_2O_2 in the inactivation process. The photocatalytic disinfection efficiency in the partition system was lower than that in the non-partition system because the life span of $^\bullet OH_{bulk}$ is extremely short and some of them may annihilate during the diffusing process [29]. This result demonstrated that direct contact between GO–ZnO composite and bacterial cell was not a prerequisite for the photocatalytic inactivation of the bacterial cells and further supported the importance of $^\bullet OH_{bulk}$ and H_2O_2 in activation process.

Since the yield of $^\bullet OH_{bulk}$ was highly dependent on the amount of H_2O_2, the concentration of H_2O_2 was directly monitored using the microplate fluorometric method [23]. As shown in Fig. 8a, the production of H_2O_2 was found to increase dramatically under VL irradiation, achieving as high as *ca.* 80 μM within 60 min, much higher than that produced by ZnO and GO (Fig. S7). Moreover, the concentration of H_2O_2 did not reach a constant value as reported previously [29,30]. In contrast, it was linearly fitted with a regression coefficient (R^2 = 0.994) within the range of 0–80 μM, demonstrating a high and continuous production of H_2O_2 by GO–ZnO composite. Surprisingly, this linear relationship was even observed after 8 h VL irradiation, with the estimated concentration of H_2O_2 to be maximum 1000 μM (R^2 = 0.965) (Fig. 8b), which far exceeded those produced by previously reported VLD photocatalysts such as $CdIn_2S_4$ (61.7 μM) [29], and Cu(II)/WO_3 (0.5 μM) [31]. Hence, the strong interaction within GO–ZnO composite maybe induce good mass production of H_2O_2, exhibiting promising potentials to H_2O_2-oriented VLD photocatalysis applications.

The contributions of $^\bullet O_2^-$ and $^\bullet OH_{bulk}$ in the VLD bacterial inactivation process were further clarified by using NBT and TA as the $^\bullet O_2^-$ and $^\bullet OH_{bulk}$ probe, respectively. NBT, exhibiting an absorption maximum at 259 nm, can directly react with $^\bullet O_2^-$ to form insoluble blue formazanb. The production was quantitatively analyzed by detecting the concentration of reduced NBT. TA readily reacts with $^\bullet OH_{bulk}$ to produce the highly fluorescent product, 2-hydroxyterephthalic acid (TAOH), which has the photoluminescence emission peak at 426 nm by excitation at 315 nm [32]. The amount of $^\bullet OH_{bulk}$ can be monitored by the fluorescence emission peak at 425 nm. As shown in Fig. 9a, the concentration of $^\bullet O_2^-$ quickly increases within 30 min and became constant with prolonged irradiation time, indicating that the generation and annihilation of $^\bullet O_2^-$ reached a dynamic equilibrium [33]. Nevertheless, the concentration of $^\bullet OH_{bulk}$ kept increasing within 60 min (Fig. 9b), which corresponded to the change trend of H_2O_2. In CB, $^\bullet O_2^-$ is formed to be activated the ambient molecular oxygen, while H_2O_2 is produced by the reduction or disproportionation of $^\bullet O_2^-$ [29], further forming $^\bullet OH_{bulk}$. Although the kinetics correlation between $^\bullet O_2^-$, $^\bullet OH_{bulk}$ and H_2O_2 is required further investigation,

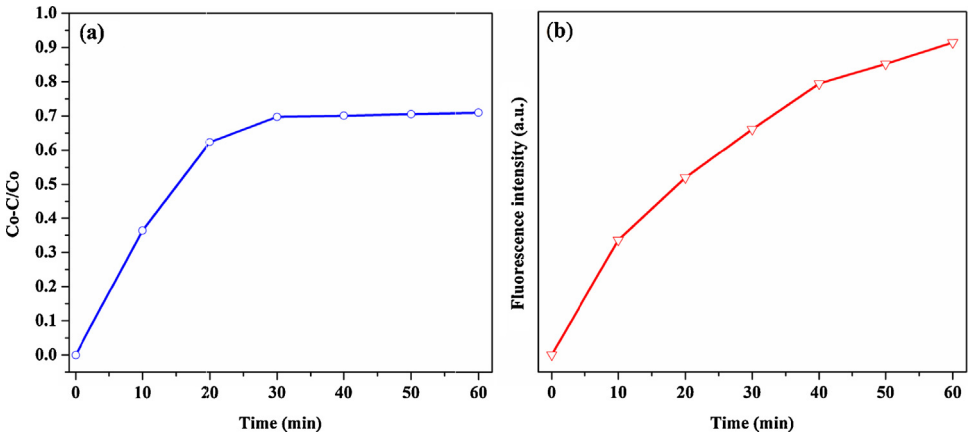

Fig. 9. (a) Transformation percentage of NBT concentration; (b) fluorescence intensity at 426 nm for TAOH with GO–ZnO composite under VL irradiation provided by fluorescence tubes.

the VLD photocatalytic bacteria inactivation of GO–ZnO composite was highly relevant to the evolution of $^{\bullet}OH_{bulk}$ and H_2O_2 rather than $^{\bullet}O_2^-$. Hence, a reliable conclusion can be drawn from above analyses that $^{\bullet}OH_{bulk}$ was the major ROS responsible for the bacterial inactivation in this case. This was also consistent with the results of scavenger study that the quenching of $^{\bullet}O_2^-$ and H_2O_2 decreased the amount of $^{\bullet}OH_{bulk}$, resulting in a significant inhibition effect on the inactivation efficiency.

Specific surface area of photocatalyst may have influence on their photocatalytic activities. Nevertheless, GO–ZnO and ZnO process similar specific surface area (Fig. S8), indicating that specific surface area of photocatalysts played neglectable effect on the significant enhancement of bacterial inactivation after GO introduction. As discussed above, the GO–ZnO composite was able to have an intense light absorption within the VL region and a more rapid interfacial charge separation and transfer under VL irradiation due to the strong interaction between GO and ZnO, but not enough to be VLD due to the wide band gap of 3.13 eV. However, when VLD photocatalytic bacterial inactivation experiment was conducted, GO–ZnO composite was found to exhibit remarkable enhancement of the activity. Finally, the above discussions guided us to infer an interaction between ZnO and GO induced VLD photocatalytic bacterial inactivation mechanism of GO–ZnO composite. The interfacial interaction between GO and the semiconductors will affect the charge carrier lifetime and transfer efficiency across the interface [34]. Accordingly, with proper interfacial interaction, the photoinduced e^- in GO can be successfully injected into the CB of semiconductors, thus producing VL activity. In fact, some theoretical calculations found that graphene can potentially act as a photosensitizer in some wide-band-gap semiconductor/graphene composites [35,36]. Therefore, GO was proposed to act as a photosensitizer in GO–ZnO composite. The conduction band minimum (E_{CBM}) potential of ZnO was calculated to be −4.39 eV *versus* a vacuum, according to the equation $E_{CBM} = \chi - E_c - 0.5E_g$, where χ is the absolute electronegativity of ZnO, E_c is the energy of free electrons on the hydrogen scale (about 4.5 eV), E_g is the band gap energy of ZnO. The potential of GO is −3.5 eV [37]. Since the energy level of GO is higher than the conduction band of ZnO, electron transfer from GO to ZnO is thermodynamically favorable. Consequently, under VL irradiation, GO was excited from the ground state to the excited state *GO, with electrons photogenerated simultaneously, which were then injected into CB of ZnO and then efficiently migrated to the surface of the GO–ZnO composite. With enhanced charge separation and transfer efficiency, these electrons activated the ambient oxygen molecules to produce highly powerful ROSs such as $^{\bullet}O_2^-$ and H_2O_2, and then resulted in $^{\bullet}OH_{bulk}$, leading to dramatically inactivation effect toward bacterial cells.

3.4. Practical application

Furthermore, the GO–ZnO composite also showed, within 10 min, a 6-log reduction of the bacterial population under natural sunlight irradiation (Fig. S9). This excellent bacterial inactivation is far exceed those of the pure TiO_2 [38], metal-doped TiO_2 [39,40], nitrogen-doped TiO_2 [40], and GO–TiO_2 [41] irradiated by sunlight. In addition to the GO photosensitizer induced effect, the UV light of the solar spectrum facilitated the utilization of the photogeneration of charges from both CB and VB of ZnO, creating a prosperous ROS-rich process for the bacterial inactivation. Thus from the viewpoint of practical application, the present work also successfully demonstrated a new and promising GO–semiconductor-based photocatalyst for the ultimate goal of solar energy utilization in water and/or wastewater purification.

4. Conclusions

In summary, GO–ZnO composite was synthesized by a simple hydrothermal method. Significantly, the obtained GO–ZnO composite exhibited superior VLD photocatalytic activity for the inactivation of *E. coli* K-12 due to the strong interaction between ZnO and GO. As GO serving as a photosensitizer, the strong interaction promoted the charge separation and transfer, resulting in boosted production of ROSs and then enhanced bacterial inactivation without direct contact with the bacteria. The $^{\bullet}OH_{bulk}$ was suggested as the major ROS responsible for the bacterial inactivation in this process. The GO–ZnO composite also showed an excellent bacterial inactivation under natural sunlight irradiation. This current study does not only provide a highly efficient VLD photocatalyst for massively H_2O_2-produced photocatalytic reactions, but also promotes further interest of GO-semiconductor photocatalyst for environmental application with the utilization of VL and sunlight.

Acknowledgements

This study was supported by a research grant (GRF476811) from the Research Grant Council of Hong Kong SAR Government to P.K. Wong, and research grants (41425015 and 21077104) from Natural Science Foundation of China to T.C. An and G.Y. Li. P.K. Wong is also supported by CAS/SAFEA International Partnership Program for Creative Research Teams of Chinese Academy of Sciences, China. The authors would like to acknowledge the technical analyses conducted at Huazhong University of Science & Technology Analytical and Testing Center.

Appendix A. Supplementary data

Supplementary data associated with this article can be found, in the online version, at http://dx.doi.org/10.1016/j.apsusc.2015.08.033

References

[1] J. Low, S. Cao, J. Yu, S. Wageh, Two-dimensional layered composite photocatalysts, Chem. Commun. 50 (2014) 10768–10777.
[2] Y.-N. Chang, X.-M. Ou, G.-M. Zeng, J.L. Gong, C.H. Deng, Y. Jiang, J. Liang, G.Q. Yuan, H.-Y. Liu, X. He, Synthesis of magnetic graphene oxide–TiO_2 and their antibacterial properties under solar irradiation, Appl. Surf. Sci. 343 (2015) 1–10.
[3] J. Zhang, L. Qi, J. Ran, J. Yu, S.Z. Qiao, Ternary NiS/$Zn_xCd_{1-x}S$/reduced graphene oxide nanocomposites for enhanced solar photocatalytic H_2-production activity, Adv. Energy Mater. 4 (2014) 1301925.
[4] P. Wang, T. Ming, G. Wang, X. Wang, H. Yu, J. Yu, Cocatalyst modification and nanonization of Ag/AgCl photocatalyst with enhanced photocatalytic performance, J. Mol. Catal. A: Chem. 381 (2014) 114–119.
[5] D. Xu, B. Cheng, S. Cao, J. Yu, Enhanced photocatalytic activity and stability of Z-scheme Ag_2CrO_4–GO composite photocatalysts for organic pollutant degradation, Appl. Catal. B: Environ. 164 (2015) 380–388.
[6] Q. Xiang, D. Lang, T. Shen, F. Liu, Graphene-modified nanosized Ag_3PO_4 photocatalysts for enhanced visible-light photocatalytic activity and stability, Appl. Catal. B: Environ. 162 (2015) 196–203.
[7] J. Low, J. Yu, Q. Li, B. Cheng, Enhanced visible-light photocatalytic activity of plasmonic Ag and graphene co-modified Bi_2WO_6 nanosheets, Phys. Chem. Chem. Phys. 16 (2014) 1111–1120.
[8] X. Pan, M.Q. Yang, Y.J. Xu, Morphology control, defect engineering and photoactivity tuning of ZnO crystals by graphene oxide – a unique 2D macromolecular surfactant, Phys. Chem. Chem. Phys. 16 (2014) 5589–5599.
[9] M. Seredych, O. Mabayoje, T.J. Bandosz, Interactions of NO_2 with zinc (hydr) oxide/graphene phase composites: visible light enhanced surface reactivity, J. Phys. Chem. C 116 (2012) 2527–2535.
[10] J. Qin, X. Zhang, Y. Xue, N. Kittiwattanothai, P. Kongsittikul, N. Rodthongkum, S. Limpanart, M. Ma, R. Liu, A facile synthesis of nanorods of ZnO/graphene oxide composites with enhanced photocatalytic activity, Appl. Surf. Sci. 321 (2014) 226–232.
[11] S. An, B.N. Joshi, M.W. Lee, N.Y. Kim, S.S. Yoon, Electrospun graphene–ZnO nanofiber mats for photocatalysis applications, Appl. Surf. Sci. 294 (2014) 24–28.
[12] Z. Hu, J. Li, C. Li, S. Zhao, N. Li, Y. Wang, F. Wei, L. Chen, Y. Huang, Folic acid-conjugated graphene–ZnO nanohybrid for targeting photodynamic therapy under visible light irradiation, J. Mater. Chem. B 1 (2013) 5003–5013.
[13] H. Sun, G. Li, X. Nie, H. Shi, P.K. Wong, H. Zhao, T. An, Systematic approach to in-depth understanding of photoelectrocatalytic bacterial inactivation mechanisms by tracking the decomposed building blocks, Environ. Sci. Technol. 48 (2014) 9412–9419.
[14] D. Wu, B. Wang, W. Wang, T. An, G. Li, T.W. Ng, H.Y. Yip, C. Xiong, H.K. Lee, P.K. Wong, Visible-light-driven BiOBr nanosheets for highly facet-dependent photocatalytic inactivation of *Escherichia coli*, J. Mater. Chem. A 3 (2015) 15148–15155.
[15] Y.-W. Wang, A. Cao, Y. Jiang, X. Zhang, J.H. Liu, Y. Liu, H. Wang, Superior antibacterial activity of zinc oxide/graphene oxide composites originating from high zinc concentration localized around bacteria, ACS Appl. Mater. Interfaces 6 (2014) 2791–2798.
[16] A. Nourmohammadi, R. Rahighi, O. Akhavan, A. Moshfegh, Graphene oxide sheets involved in vertically aligned zinc oxide nanowires for visible light photoinactivation of bacteria, J. Alloys Compd. 612 (2014) 380–385.
[17] P. Song, X. Zhang, M. Sun, X. Cui, Y. Lin, Graphene oxide modified TiO_2 nanotube arrays: enhanced visible light photoelectrochemical properties, Nanoscale 4 (2012) 1800–1804.
[18] Q. Xiang, B. Cheng, J. Yu, Graphene-based photocatalysts for solar-fuel generation, Angew. Chem. Int. Ed. Engl. (2015), http://dx.doi.org/10.1002/anie.201411096
[19] Y. Zhang, N. Zhang, Z.-R. Tang, Y.J. Xu, Graphene transforms wide band gap ZnS to a visible light photocatalyst. The new role of graphene as a macromolecular photosensitizer, ACS Nano 6 (2012) 9777–9789.
[20] P. Zeng, Q. Zhang, X. Zhang, T. Peng, Graphite oxide–TiO_2 nanocomposite and its efficient visible-light-driven photocatalytic hydrogen production, J. Alloys Compd. 516 (2012) 85–90.
[21] X. Bai, L. Wang, Y. Zhu, Visible photocatalytic activity enhancement of $ZnWO_4$ by graphene hybridization, ACS Catal. 2 (2012) 2769–2778.
[22] D.C. Marcano, D.V. Kosynkin, J.M. Berlin, A. Sinitskii, Z. Sun, A. Slesarev, L.B. Alemany, W. Lu, J.M. Tour, Improved synthesis of graphene oxide, ACS Nano 4 (2010) 4806–4814.
[23] M. Abbas, W. Luo, L. Zhu, J. Zou, H. Tang, Fluorometric determination of hydrogen peroxide in milk by using a Fenton reaction system, Food Chem. 120 (2010) 327–331.
[24] O. Akhavan, Photocatalytic reduction of graphene oxides hybridized by ZnO nanoparticles in ethanol, Carbon 49 (2011) 11–18.
[25] Z. Sun, C. Yang, M. Liu, C. Chen, S. Xu, C. Zhang, B. Man, Limited graphene oxidation on the synthesis of ZnO–graphene hybrid nanostructures by the Zn predeposition, Appl. Surf. Sci. 315 (2014) 368–371.
[26] H. Shi, G. Li, H. Sun, T. An, H. Zhao, P.-K. Wong, Visible-light-driven photocatalytic inactivation of *E. coli* by Ag/AgX-CNTs (X = Cl, Br, I) plasmonic photocatalysts: Bacterial performance and deactivation mechanism, Appl. Catal. B: Environ. 158 (2014) 301–307.
[27] F. Bosshard, M. Bucheli, Y. Meur, T. Egli, The respiratory chain is the cell's Achilles' heel during UVA inactivation in *Escherichia coli*, Microbiology 156 (2010) 2006–2015.
[28] J. Zhao, Z. Wang, Y. Dai, B. Xing, Mitigation of CuO nanoparticle-induced bacterial membrane damage by dissolved organic matter, Water Res. 47 (2013) 4169–4178.
[29] W. Wang, T.W. Ng, W.K. Ho, J. Huang, S. Liang, T. An, G. Li, C.Y. Jimmy, P.K. Wong, $CdIn_2S_4$ microsphere as an efficient visible-light-driven photocatalyst for bacterial inactivation: synthesis, characterizations and photocatalytic inactivation mechanisms, Appl. Catal. B: Environ. 129 (2013) 482–490.
[30] D. Xia, T.W. Ng, T. An, G. Li, Y. Li, H.Y. Yip, H. Zhao, A. Lu, P.K. Wong, A recyclable mineral catalyst for visible-light-driven photocatalytic inactivation of bacteria: natural magnetic sphalerite, Environ. Sci. Technol. 47 (2013) 11166–11173.
[31] Y. Nosaka, S. Takahashi, H. Sakamoto, A.Y. Nosaka, Reaction mechanism of Cu (II)-grafted visible-light responsive TiO_2 and WO_3 photocatalysts studied by means of ESR spectroscopy and chemiluminescence photometry, J. Phys. Chem. C 115 (2011) 21283–21290.
[32] L. Zhang, L. Du, X. Yu, S. Tan, X. Cai, P. Yang, Y. Gu, W. Mai, Significantly enhanced photocatalytic activities and charge separation mechanism of Pd-decorated ZnO–graphene oxide nanocomposites, ACS Appl. Mater. Interfaces 6 (2014) 3623–3629.
[33] X. Qu, P.J. Alvarez, Q. Li, Photochemical transformation of carboxylated multiwalled carbon nanotubes: role of reactive oxygen species, Environ. Sci. Technol. 47 (2013) 14080–14088.
[34] M.-Q. Yang, Y.-J. Xu, Basic principles for observing the photosensitizer role of graphene in the graphene–semiconductor composite photocatalyst from a case study on graphene–ZnO, J. Phys. Chem. C 117 (2013) 21724–21734.
[35] R. Long, N.J. English, O.V. Prezhdo, Photo-induced charge separation across the graphene–TiO_2 interface is faster than energy losses: a time-domain ab initio analysis, J. Am. Chem. Soc. 134 (2012) 14238–14248.
[36] A. Du, S. Sanvito, Z. Li, D. Wang, Y. Jiao, T. Liao, Q. Sun, Y.H. Ng, Z. Zhu, R. Amal, Hybrid graphene and graphitic carbon nitride nanocomposite: gap opening, electron–hole puddle, interfacial charge transfer, and enhanced visible light response, J. Am. Chem. Soc. 134 (2012) 4393–4397.
[37] T.F. Yeh, J.M. Syu, C. Cheng, T.H. Chang, H. Teng, Graphite oxide as a photocatalyst for hydrogen production from water, Adv. Funct. Mater. 20 (2010) 2255–2262.
[38] M. Ortega-Liébana, E. Sánchez-López, J. Hidalgo-Carrillo, A. Marinas, J. Marinas, F. Urbano, A comparative study of photocatalytic degradation of 3-chloropyridine under UV and solar light by homogeneous (photo-Fenton) and heterogeneous (TiO_2) photocatalysis, Appl. Catal. B: Environ. 127 (2012) 316–322.
[39] D. Venieri, A. Fraggedaki, M. Kostadima, E. Chatzisymeon, V. Binas, A. Zachopoulos, G. Kiriakidis, D. Mantzavinos, Solar light and metal-doped TiO_2 to eliminate water-transmitted bacterial pathogens: photocatalyst characterization and disinfection performance, Appl. Catal. B: Environ. 154 (2014) 93–101.
[40] M.B. Fisher, D.A. Keane, P. Fernandez-Ibanez, J. Colreavy, S.J. Hinder, K.G. McGuigan, S.C. Pillai, Nitrogen and copper doped solar light active TiO_2 photocatalysts for water decontamination, Appl. Catal. B: Environ. 130 (2013) 8–13.
[41] O. Akhavan, E. Ghaderi, Photocatalytic reduction of graphene oxide nanosheets on TiO_2 thin film for photoinactivation of bacteria in solar light irradiation, J. Phys. Chem. C 113 (2009) 20214–20220.